Autophagic clearance of proteasomes in yeast requires the conserved sorting nexin Snx4

Received for publication, September 15, 2017, and in revised form, November 3, 2017 Published, Papers in Press, November 6, 2017, DOI 10.1074/jbc.M117.817999

Antonia A. Nemec[1], **Lauren A. Howell**[1], **Anna K. Peterson, Matthew A. Murray, and Robert J. Tomko Jr.**[2]

From the Department of Biomedical Sciences, College of Medicine, Florida State University, Tallahassee, Florida 32306

Edited by George N. DeMartino

Turnover of the 26S proteasome by autophagy is an evolutionarily conserved process that governs cellular proteolytic capacity and eliminates inactive particles. In most organisms, proteasomes are located in both the nucleus and cytoplasm. However, the specific autophagy routes for nuclear and cytoplasmic proteasomes are unclear. Here, we investigate the spatial control of autophagic proteasome turnover in budding yeast (*Saccharomyces cerevisiae*). We found that nitrogen starvation–induced proteasome autophagy is independent of known nucleophagy pathways but is compromised when nuclear protein export is blocked. Furthermore, via pharmacological tethering of proteasomes to chromatin or the plasma membrane, we provide evidence that nuclear proteasomes at least partially disassemble before autophagic turnover, whereas cytoplasmic proteasomes remain largely intact. A targeted screen of autophagy genes identified a requirement for the conserved sorting nexin Snx4 in the autophagic turnover of proteasomes and several other large multisubunit complexes. We demonstrate that Snx4 cooperates with sorting nexins Snx41 and Snx42 to mediate proteasome turnover and is required for the formation of cytoplasmic proteasome puncta that accumulate when autophagosome formation is blocked. Together, our results support distinct mechanistic paths in the turnover of nuclear *versus* cytoplasmic proteasomes and point to a critical role for Snx4 in cytoplasmic agglomeration of proteasomes *en route* to autophagic destruction.

In eukaryotes, two main pathways exist for the regulated destruction of proteins: macroautophagy (hereafter autophagy) and the ubiquitin–proteasome system (UPS)[3] (1). The UPS catalyzes the ubiquitin-dependent degradation of protein substrates by the proteasome, a highly conserved 2.5-MDa multisubunit ATP-dependent protease complex (2, 3). The proteasome consists of a barrel-shaped proteolytic core particle (CP) that houses the peptidase active sites in its interior. The CP can be capped on one or both ends by the 19S regulatory particle (RP). The RP can be further divided into lid and base subcomplexes. The lid contains an enzymatic activity that removes the polyubiquitin targeting signal from the substrate. The base contains a ring of AAA^+ family ATPases that use mechanical force derived from ATP to unfold the substrate and translocate it into the interior of the CP for destruction.

In contrast to the UPS, autophagy comprises the engulfment of cellular contents in a double-membraned vesicle called an autophagosome for delivery to and destruction in the lysosome (vacuole in yeasts) (4). In the canonical non-selective form of autophagy, a portion of the cytoplasm is delivered in bulk to the vacuole for destruction. This process is directed by the covalent attachment of the small ubiquitin-like protein, Atg8, onto growing autophagosomal membranes to promote membrane expansion and subsequent engulfment of cellular components. Fusion of the autophagosome with the vacuolar membrane delivers the contents into the vacuolar lumen, where the contents are destroyed by various hydrolases. Whereas the UPS can recycle only proteins, autophagy can recycle proteins, lipids, and nucleic acids (5, 6). Furthermore, because substrates are typically encapsulated *en masse* in the cytosol, autophagy is better suited than the UPS for the destruction of exceptionally large or complicated cargoes, such as organelles (7), pathogenic organisms (8), or multisubunit complexes (9–11).

In addition to the canonical non-selective (bulk) autophagy, individual cargoes can be earmarked for turnover by autophagy in a process termed selective autophagy. Selective autophagy has recently emerged as a critical homeostatic paradigm and is deregulated in numerous human diseases (12). In selective autophagy, a particular cargo is typically recruited to the assembling autophagosomal membrane, called the phagophore assembly site (PAS), via a cargo-selective autophagy receptor. This receptor binds both the substrate and Atg8-coated PAS membrane to promote cargo engulfment (13).

The selective autophagic turnover of the proteasome has recently been demonstrated in mammals (14), plants (15), and in the budding yeast *Saccharomyces cerevisiae* (16, 17) and occurs in response to nitrogen starvation or treatment of cells with proteasome inhibitors. This conserved pathway serves to control both the abundance and the quality of proteasomes to preserve organismal health. In response to the proteasome

This work was supported by start-up funds from the Florida State University College of Medicine and National Institutes of Health Grant 1R01GM118600 from NIGMS (to R. J. T., Jr.). The content is solely the responsibility of the authors and does not necessarily represent the official views of the National Institutes of Health. The authors declare that they have no conflicts of interest with the contents of this article. The content is solely the responsibility of the authors and does not necessarily represent the official views of the National Institutes of Health.

This article contains supplemental Tables 1 and 2.

[1] Both authors contributed equally to this work.

[2] To whom correspondence should be addressed: 1115 W. Call St., Tallahassee, FL 32306. Tel.: 850-645-1482; E-mail: robert.tomko@med.fsu.edu.

[3] The abbreviations used are: UPS, ubiquitin–proteasome system; BAR, Bin/amphiphysin/Rvs; CP, core particle; CVT, cytoplasm-to-vacuole targeting; FAS, fatty-acid synthase; PAS, phagophore assembly site; PI3P, phosphatidylinositol 3-phosphate; PM, plasma membrane; PMN, piecemeal autophagy of the nucleus; PX, phox homology; RP, regulatory particle; ANOVA, analysis of variance; suc, succinyl; AMC, amido-4-methylcoumarin; ER, endoplasmic reticulum.

inhibitor MG132, proteasomes undergo ubiquitination-dependent delivery to the autophagosome by the autophagy receptor Cue5. The selective recognition of proteasomes for autophagy in response to nitrogen starvation is thus far poorly understood but appears to involve distinct paths for the RP and CP subcomplexes, based in part on differential requirements for the ubiquitin protease Ubp3 for delivery of RP and CP subunits to the vacuole (17).

For both proteasome inhibitor-triggered and nitrogen starvation–induced proteasome autophagy, formation of cytoplasmic puncta that are apparently distinct from the PAS precedes delivery to the vacuole. In response to the chemical proteasome inhibitor MG132, proteasomes destined for autophagic turnover colocalize with markers of insoluble protein deposits (16), whereas in nitrogen-starved cells unable to form the PAS due to deletion of *ATG17,* proteasomes form cytoplasmic puncta of unknown origin or composition (17). Together, these observations suggest that proteasomes may be concentrated or encapsulated prior to their delivery to the PAS, but the mechanism(s) and mediator(s) of this cytoplasmic agglomeration are unknown.

One potential barrier to the recruitment of proteasomes to the PAS is that a substantial proportion of proteasomes is located in the nucleus in yeasts (18, 19) and in many mammalian cells (20–22), whereas encapsulation of cargo by the growing autophagosome occurs solely in the cytosol. Very little is known about autophagy of nuclear components. In mammals, autophagy of the nuclear lamina has been reported (23). In budding yeast, a pathway called piecemeal autophagy of the nucleus (PMN) has been shown to dispose of nuclear components via direct engulfment of nuclear blebs by the vacuole. This process requires the formation of nucleus–vacuole junctions via Nvj1 (24) and Lam6 (and potentially its homolog Lam5) (25). More recently, selective autophagy of nuclear components was shown to be mediated by the receptor Atg39 (26). This Atg39-dependent nucleophagy appears to be distinct from PMN. The mechanism by which nuclear proteasomes may be turned over by autophagy, as well as the relative contributions of these known forms of nucleophagy, remains unclear.

The proteasome, the core autophagy machinery, and autophagic proteasome turnover are each highly conserved from yeasts to humans. Budding yeast therefore serves as an excellent model both for probing the pathway(s) and mediators of proteasome autophagy, as well as for unveiling conserved mechanistic underpinnings of selective autophagy. In this study, we utilize this highly tractable model eukaryote to investigate how proteasomes are sourced and packaged for destruction in the vacuole via selective autophagy. Our data support a model of distinct mechanistic paths for nuclear *versus* cytoplasmic proteasomes, in which nuclear proteasomes are disassembled in the nucleus prior to autophagy. Furthermore, our data suggest that proteasomes transiently accumulate in cytoplasmic puncta in a manner dependent on the conserved sorting nexins Snx4/41/42 before Atg8-dependent delivery to the vacuole for destruction. Finally, we show that Snx4 dependence for autophagy is shared with at least two other soluble multisubunit complexes. In summary, our study clarifies selective autophagy of proteasomes and unveils a requirement for sorting nexins in autophagy of diverse multisubunit complexes.

Results

Proteasome autophagy requires nuclear export and is independent of known forms of nuclear autophagy

To determine whether known forms of nucleophagy mediate the destruction of proteasomes, we first created a yeast strain expressing green fluorescent protein (GFP)-tagged α4 core particle subunit (Fig. 1*A*), encoded by the *PRE6* gene, from its chromosomal locus. In yeast, delivery of GFP-fused proteins to the vacuole via autophagy releases a 27-kDa GFP fragment that is resistant to proteolysis and can be readily detected via GFP immunoblotting (27). The α4-GFP protein was found in fully assembled CP and in CP capped with regulatory particles (RP_2CP and RP_1CP), as gauged by in-gel GFP fluorescence imaging of proteasomes in whole-cell extracts via native PAGE (Fig. 1*B*). These proteasomes were proteolytically active, as inferred from the cleavage of the well-characterized fluorogenic peptidase substrate suc-LLVY-AMC (Fig. 1*B*). This α4-GFP protein fusion was efficiently delivered to the vacuole upon nitrogen starvation as gauged by accumulation of a GFP fragment on immunoblots, and this process was compromised in cells lacking the core autophagy gene *ATG8* or the main vacuolar protease *PEP4* (detailed below in Figs. 3, 4, and 6), confirming the GFP fragment results from autophagy. We next introduced the chromosomal *PRE6-GFP* allele into a panel of yeast strains lacking genes known to be required for PMN (*NVJ1, LAM5*, and *LAM6*) or Atg39-dependent nucleophagy (24–26). To our surprise, none of the tested strains were appreciably compromised for α4-GFP autophagy (Fig. 1*C*), indicating that proteasomes were turned over independent of PMN or Atg39-dependent nucleophagy.

The nuclear pore complex mediates the bulk of nucleocytoplasmic traffic, and most proteins are exported from the nucleus via the exportin Crm1. To test a role for nuclear export in proteasome autophagy, we exploited a well-characterized temperature-sensitive *CRM1* allele, *xpo1-1*, that is near-completely defective for Crm1-dependent nuclear export at 37 °C (28). Because the core autophagy machinery is located in the cytosol (4), we anticipated that blockade of nuclear export would not globally impair autophagy over our experimental time course. To test this, we monitored nitrogen starvation–induced cleavage of GFP-Atg8, a widely accepted marker of autophagic flux (27), at the permissive (25 °C) or non-permissive (37 °C) temperature. Although blockade of nuclear export was maintained for at least 12 h (Fig. 1*D*), no appreciable difference in GFP accumulation from GFP-Atg8 was observed, even after prolonged incubation of *xpo1-1* cells at the non-permissive temperature (Fig. 1*E*). Thus, as anticipated, the cytosolic autophagy machinery remained intact upon disruption of nuclear export, at least over our experimental time course.

We next tested the effect of blocking nuclear export on autophagic turnover of GFP-tagged proteasome subunits. As we did for α4, we generated strains expressing GFP-tagged alleles of the lid subunit Rpn5 and the base subunit Rpn2 from their chromosomal loci as reporters for these subcomplexes

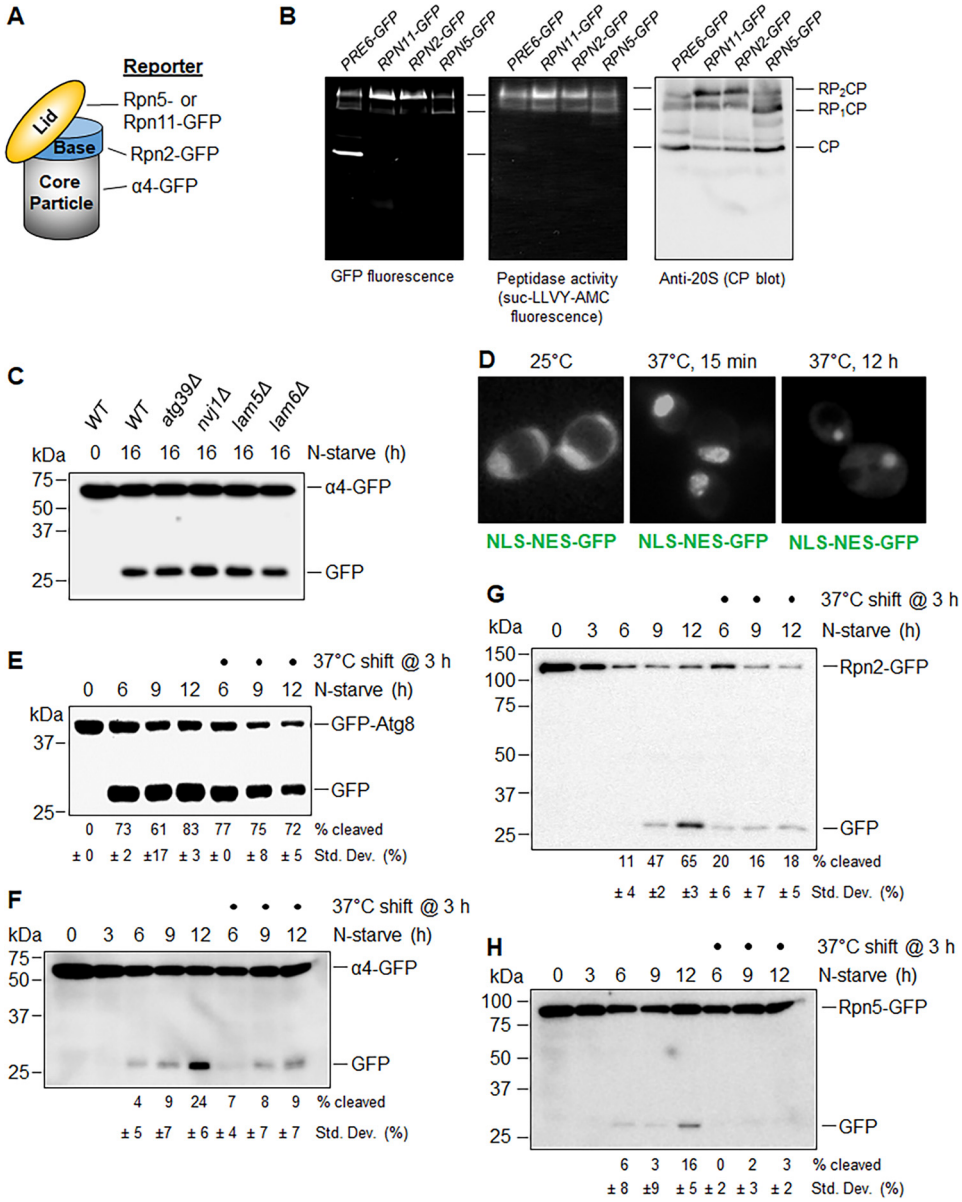

Figure 1. Proteasome autophagy is independent of known nucleophagy genes and is impaired by blockade of nuclear export. *A,* proteasome subunit-GFP fusion autophagy reporters used in Fig. 1. Rpn5 and Rpn11 are subunits of the lid subcomplex, Rpn2 of the base subcomplex, and α4 of the core particle subcomplex. *B,* whole-cell extracts of the indicated strains expressing proteasome subunits as GFP fusions from their chromosomal loci were prepared under non-denaturing conditions and separated by non-denaturing PAGE before in-gel imaging of GFP fluorescence (*left*), peptidase activity (*middle*), or immunoblotting with antibodies against the core particle (*right*). Uncapped CP displays comparatively weak peptidase activity because of restricted access of the substrate to the peptidase sites in the absence of the RP. *C,* indicated strains were subjected to nitrogen starvation for the indicated times, followed by immunoblotting of cell extracts with anti-GFP antibodies. *D,* cells containing the *xpo1-1* nuclear export mutation and expressing a nucleocytoplasmic shuttling reporter, NLS-NES-GFP (where NLS is nuclear localization signal, and NES is nuclear export signal), were incubated in log phase at 25 °C before shifting to 37 °C for 15 min or 12 h as shown. *E–H,* cells harboring the *xpo1-1* conditional nuclear export mutant allele and expressing GFP-Atg8 (*E*), α4-GFP (*F*), Rpn2-GFP (*G*), or Rpn5-GFP (*H*) were grown at permissive temperature in rich media and then transferred to SD-N medium. After 3 h, the cells were either shifted to 37 °C (*black circles*) or left at 25 °C before harvest at the indicated times for immunoblotting of cell extracts with antibodies against GFP. The percentage of GFP fragment is shown as % cleaved ± S.D. ($n \geq 3$).

(Fig. 1*A*). As for the α4-GFP fusion, both Rpn5-GFP and Rpn2-GFP were near-fully incorporated into proteolytically active 26S proteasomes (RP_2CP and RP_1CP) based on in-gel GFP fluorescence imaging of proteasomes in whole-cell extracts separated by non-denaturing PAGE and peptidase assay (Fig. 1*B*).

We then introduced these three alleles individually into the *xpo1-1* mutant background. At the permissive temperature, we observed a time-dependent increase in free GFP cleaved from α4-GFP (Fig. 1*F*) in *xpo1-1* cells upon nitrogen starvation. In contrast, GFP accumulation was significantly attenuated at the non-permissive temperature, although some small amount of GFP accumulated in these cells. This GFP signal may be derived from proteasomes that were already cytoplasmic at the time of the temperature shift, as nuclear export blockade remained largely intact over our time course (Fig. 1*D*). We observed similar results when a subunit of the base (Rpn2-GFP, Fig. 1*G*) or lid (Rpn5-GFP, Fig. 1*H*) was tested. Rpn11 has previously been reported to interact physically with Crm1 (29). However,

despite extensive efforts, we were unable to copurify proteasome subunits of the lid, base, or CP with Crm1 (data not shown). Although we cannot exclude the possibility that interaction with Crm1 was too transient or labile to detect under our experimental conditions, we suggest that failed autophagy of proteasome subunits in the *xpo1-1* mutant may potentially reflect the failed export of some other essential factor(s) rather than of proteasome subunits themselves. Regardless, because bulk autophagy was not impaired by blockade of nuclear export (Fig. 1*E*), and because autophagy of proteasomes was compromised (Fig. 1, *F–H*), we conclude that Crm1-dependent nuclear export of an as-yet unknown factor(s) is required for efficient autophagy of proteasomes.

Subcellular tethering of proteasomal subcomplexes provides evidence for disassembly in the nucleus prior to autophagy

We next sought to ask whether nuclear proteasomes exit the nucleus intact or whether they instead can be disassembled prior to nuclear egress. Conflicting reports exist on whether proteasomes disassemble prior to autophagy (16, 17). Both of these studies investigated the proteasome assembly state in whole-cell extracts that presumably contained mixtures of nuclear and cytoplasmic proteasomes, confounding analysis of a particular subcellular proteasome population. To circumvent this limitation, we utilized the anchor-away approach (30) to enrich or deplete proteasomes from the nucleus. The anchor-away approach affords control over the subcellular localization of a protein of interest by inducibly tethering it to an "anchor" protein that is invariantly located either in the cytoplasm or the nucleus.

We reasoned that if proteasomes must exit the nucleus intact, then trapping one subcomplex of the proteasome, such as the lid, in the nucleus would prevent autophagy of base or CP subunits. Alternatively, if the base and/or CP is able to dissociate from the lid prior to nuclear egress, then such trapping would have no effect (Fig. 2*A*). We utilized two anchors as follows: the histone Htb2, which localizes exclusively to the nucleus as part of chromatin; and the plasma membrane protein Pma1, which localizes specifically to the plasma membrane. Importantly, we confirmed that Htb2 is not turned over by autophagy in response to nitrogen starvation (Fig. 2*B*), and others have demonstrated the same for Pma1 (31).

We introduced chromosomal alleles encoding α4-GFP or Rpn2-GFP into cells expressing lid subunit Rpn11 as a fusion to mCherry and the rapamycin-binding FRB domain (Rpn11-FRB-mCherry). The mCherry tag allowed for visual confirmation of rapamycin-dependent subcellular tethering. These strains also expressed either a nuclear (Htb2-FKBP12) or plasma membrane (PM) (Pma1–2xFKBP12) anchor protein fusion (Fig. 2*A*). In this way, addition of rapamycin tethers Rpn11-FRB-mCherry either to chromatin or to the cytosolic face of the PM. Although rapamycin can induce autophagy via inhibition of Tor1 in WT cells, the rapamycin-insensitive *TOR1-1* mutation in the anchor-away cells rendered them insensitive to rapamycin-induced autophagy (Fig. 2*C*), and thus rapamycin treatment did not interfere with our approach.

As expected, addition of DMSO alone or addition of rapamycin to cells lacking an anchor protein had no effect on the localization of Rpn11-FRB-mCherry or α4-GFP (Fig. 2*D*, compare *panels i–vi*). Rapamycin addition to the nuclear anchor strain enriched Rpn11-FRB-mCherry and α4-GFP in the nucleus (Fig. 2*D*, *panels vii–xii*), whereas rapamycin addition to the PM anchor strain depleted these proteins from the nucleus (Fig. 2*D*, *panels xiii–xviii*). This relocalization occurred rapidly and was maintained for at least 24 h in nitrogen-starved cells (Fig. 2*D*). Thus, our anchor system effectively relocalized proteasomes to or from the nucleus under nitrogen starvation conditions. Furthermore, the relocalization of much of the α4-GFP signal along with Rpn11-FRB-mCherry upon rapamycin treatment indicates that the majority of proteasomes are fully assembled *in vivo*, consistent with previous reports (32).

We then pretreated cells harboring the nuclear or PM anchor with rapamycin to induce tethering and then induced autophagy via nitrogen starvation. We then monitored the release of GFP fragment from α4-GFP or Rpn2-GFP as a measure of delivery to the vacuole. Importantly, no compromise of α4-GFP (Fig. 2*E*, *left panel*) or Rpn2-GFP (Fig. 2*F*, *left panel*) cleavage was observed upon tethering of Rpn11 to the chromatin, even though Rpn11 was nearly completely nucleus-based on mCherry fluorescence (Fig. 2*D*, *panels vii–xii*). This strongly suggests that in nuclear proteasomes targeted for autophagy, the CP and the base can dissociate from the lid prior to nuclear egress. In contrast, tethering of Rpn11 to the plasma membrane compromised autophagy of both α4 (Fig. 2*E*, *right panel*) and Rpn2 (Fig. 2*F*, *right panel*). This result further confirms that rapamycin-induced tethering was effective under our experimental conditions and strengthens our conclusion that proteasomes can be disassembled prior to nuclear export for autophagy. Importantly, our finding that autophagy of proteasome subunits Rpn2 and α4 was compromised when Rpn11 was tethered to the cell periphery suggests that disassembly precedes destruction for nuclear but not cytoplasmic proteasomes.

Targeted genetic screen identifies a requirement for the conserved sorting nexin Snx4 in proteasome autophagy

Because known forms of nucleophagy were dispensable for α4-GFP autophagy, we next performed a targeted screen to identify the full complement of *ATG* gene products required for turnover of proteasomes upon nitrogen starvation. We picked each of the known *ATG* gene knock-out strains from the yeast knock-out library (33) to create a targeted autophagy system knock-out library. We then introduced the chromosomal *PRE6-GFP* allele into this library via standard yeast genetic array methodology (34), allowing us to search for strains that failed to accrue the diagnostic GFP cleavage fragment from α4-GFP upon nitrogen starvation. As anticipated, deletion of *ATG* genes encoding the core autophagy machinery (*ATG1–10, ATG12–16,* and *ATG18*) or *ATG* genes that are specifically required for nitrogen starvation–induced autophagy (*ATG17, ATG29,* and *ATG31*) completely abolished cleavage of α4-GFP (Fig. 3). In contrast, α4-GFP autophagy was retained in nearly all strains harboring deletions of other *ATG* genes, with the sole exception being deletion of *ATG24* (standard name and hereafter *SNX4*), which completely compromised cleavage of α4-GFP (Fig. 3). We thus focused our further efforts on *SNX4*.

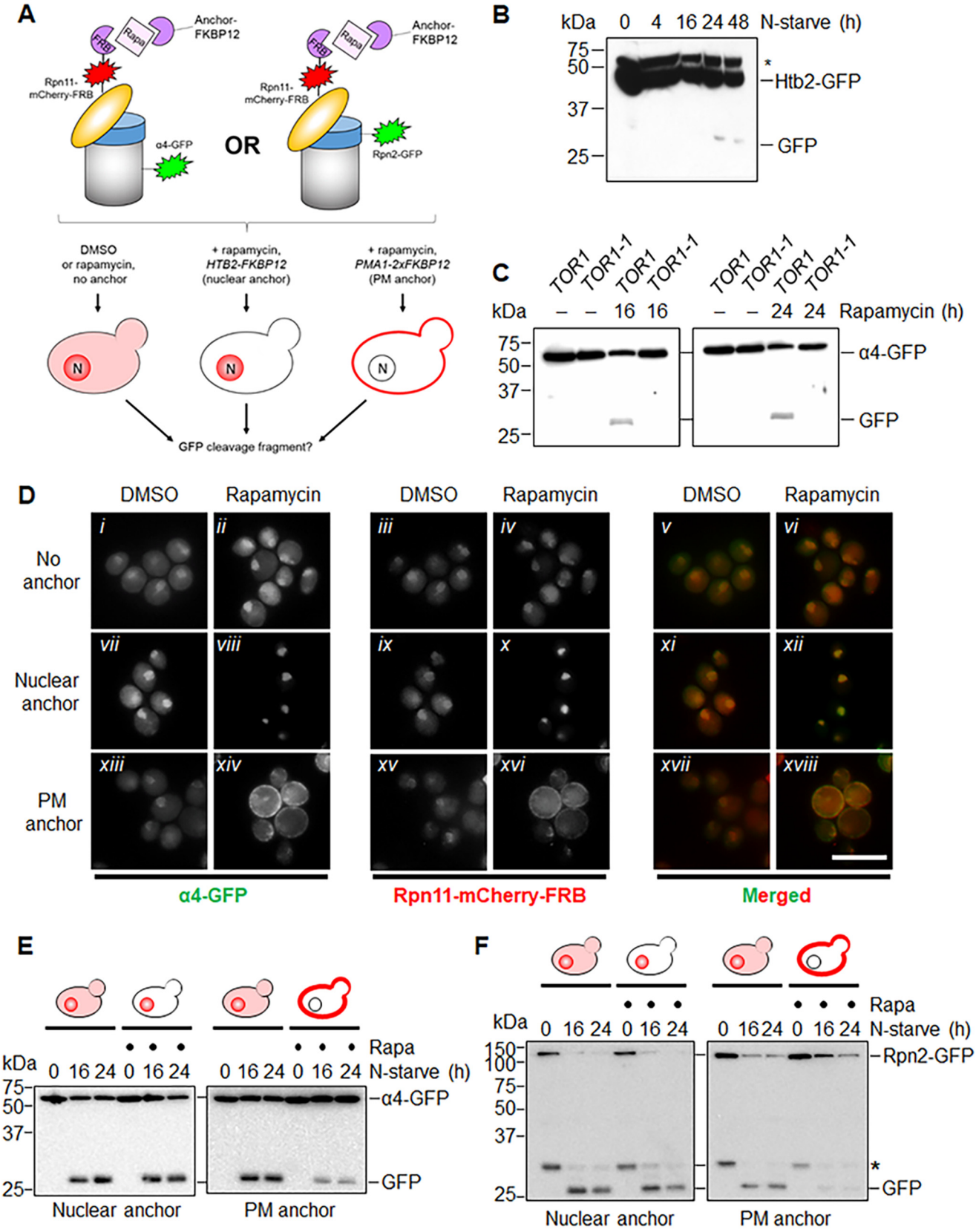
A
Anchor-FKBP12
Rapa
FRB
Rpn11-mCherry-FRB
α4-GFP
OR
Rpn2-GFP
DMSO or rapamycin, no anchor
+ rapamycin, HTB2-FKBP12 (nuclear anchor)
+ rapamycin, PMA1-2xFKBP12 (PM anchor)
N
GFP cleavage fragment?
B
kDa 0 4 16 24 48 N-starve (h)
75
50
37
25
Htb2-GFP
GFP
C
TOR1 TOR1-1 TOR1 TOR1-1 TOR1 TOR1-1 TOR1 TOR1-1
kDa – – 16 16 – – 24 24 Rapamycin (h)
75
50
37
25
α4-GFP
GFP
D
DMSO Rapamycin DMSO Rapamycin DMSO Rapamycin
No anchor
Nuclear anchor
PM anchor
i ii iii iv v vi
vii viii ix x xi xii
xiii xiv xv xvi xvii xviii
α4-GFP
Rpn11-mCherry-FRB
Merged
E
Rapa
kDa 0 16 24 0 16 24 0 16 24 0 16 24 N-starve (h)
75
50
37
25
α4-GFP
GFP
Nuclear anchor
PM anchor
F
Rapa
kDa 0 16 24 0 16 24 0 16 24 0 16 24 N-starve (h)
150
100
75
50
37
25
Rpn2-GFP
*
GFP
Nuclear anchor
PM anchor

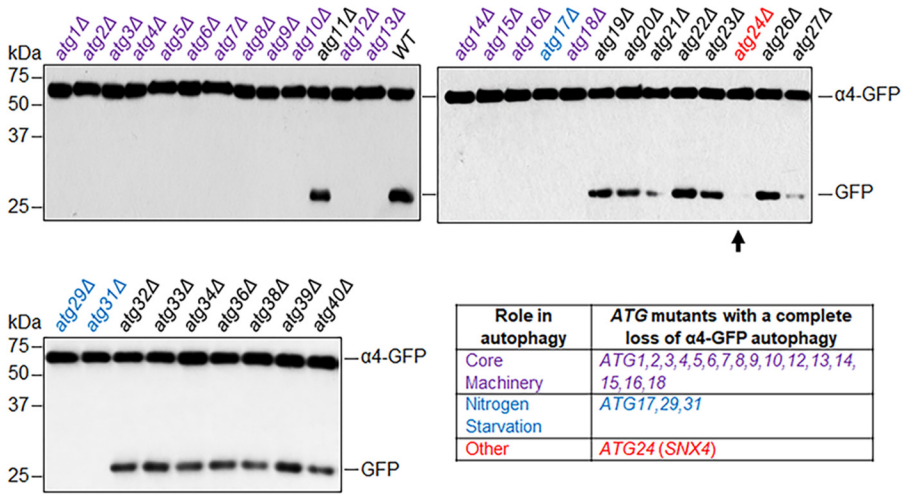

Role in autophagy	*ATG* mutants with a complete loss of α4-GFP autophagy
Core Machinery	*ATG1,2,3,4,5,6,7,8,9,10,12,13,14, 15,16,18*
Nitrogen Starvation	*ATG17,29,31*
Other	*ATG24 (SNX4)*

Figure 3. Targeted genetic screen to define *ATG* genes required for proteasome autophagy. The indicated strains were nitrogen-starved for 16 h before harvesting for immunoblotting of whole-cell extracts with anti-GFP antibodies. An *arrowhead* highlights the complete loss of autophagy in the *atg24*Δ (*snx4*Δ) strain. *Inset table,* description of the autophagy-specific functions of genes that, when deleted, demonstrated a complete loss of GFP formation. Genes encoding components of the core autophagy machinery are listed in *purple* both in the immunoblots and in the *table*. Genes specific to nitrogen starvation are shown in *blue*, and *ATG24/SNX4* is shown in *red*.

SNX4 encodes a member of the sorting nexin containing a Bin/amphiphysin/Rvs (BAR) domain (SNX-BAR) protein family and has obvious orthologs in most eukaryotes, including yeasts and humans (35). SNX-BAR proteins typically contain an N-terminal Phox homology (PX) domain that binds phosphatidylinositol 3-phosphate (PI3P), and a C-terminal BAR domain that promotes association with membranes of defined curvature (36). PI3P is enriched on endosomal membranes, and this association with curved PI3P-containing membranes drives formation of highly tubulated endosomal microdomains for cargo enrichment that then bud off for subsequent cargo transport. In addition to its roles in endosomal sorting (37–41), Snx4 has previously been implicated in the autophagy of mitochondria, peroxisomes, and ER (10, 42–45) and in the budding yeast-specific cytoplasm-to-vacuole targeting (CVT) pathway (44), which delivers a select number of resident enzymes to the vacuole in a manner mechanistically similar to selective autophagy. However, the functional mechanism(s) of Snx4 in these processes, as well as its contributions to other forms of selective autophagy, are poorly defined.

To better understand how Snx4 regulates autophagy of proteasomes, we first tested whether deletion of *SNX4* was simply slowing α4-GFP turnover or instead was compromising it completely. We measured the time-dependent accumulation of cleaved GFP in nitrogen-starved WT and *snx4*Δ cells and in *atg8*Δ cells as a control for general compromise of autophagy. As was the case in *atg8*Δ cells, no detectable accumulation of GFP was observed in *snx4*Δ cells, even after prolonged nitrogen starvation (Fig. 4*A*). Deletion of *SNX4* similarly compromised turnover of the base subunit Rpn2-GFP and the lid subunit Rpn5-GFP (Fig. 4*B*), suggesting that Snx4 is required for turnover of all three proteasomal subcomplexes: lid, base, and CP.

Proteasome autophagy has been demonstrated recently in response to treatment of cells with the proteasome inhibitor MG132 (15, 16). We therefore asked whether Snx4 function was required for turnover of proteasomes in response to MG132. We used cells harboring a deletion in the ATP-binding cassette transporter *PDR5* to enhance intracellular accumulation of MG132 by reducing drug efflux (46). As was previously reported (16), MG132 induced autophagy of proteasomes, as evidenced by accumulation of the diagnostic GFP proteolytic fragment (Fig. 4*C*). In contrast to reports by others (15, 16), neither MG132 nor the clinically used proteasome inhibitor bortezomib (data not shown) robustly induced autophagy of proteasomes in our hands; this may result in part from our use of a *PDR5* deletion to enhance uptake of these small molecules

Figure 2. Nuclear proteasomes can disassemble prior to autophagy. *A,* experimental scheme to test whether proteasomal subcomplexes can disassemble prior to autophagy. Rpn2-GFP or α4-GFP was expressed from the chromosomal locus in tether-anchor strains harboring chromosomal *RPN11-mCherry-FRB* (tether) and either no anchor, *HTB2*-FKBP12, or *PMA1–2xFKBP12* alleles. The strains were then treated with DMSO vehicle or with 1 μg/ml rapamycin, followed by nitrogen starvation for different time periods before examination of GFP cleavage by immunoblotting. *B*, histone Htb2-GFP is not appreciably turned over by autophagy in response to nitrogen starvation. Yeast expressing Htb2-GFP from the chromosomal locus were nitrogen-starved for the indicated time periods before harvesting. Cell extracts were separated via SDS-PAGE and subjected to immunoblotting with anti-GFP antibodies. An *asterisk* indicates post-translationally modified Htb2-GFP. The blot was intentionally overexposed to emphasize that essentially no free GFP was released upon nitrogen starvation. *C*, cells harboring WT *TOR1* or the rapamycin-insensitive *TOR1-1* allele were treated with DMSO vehicle or 1 μg/ml rapamycin for the indicated times. Cell extracts from treated cells were then subjected to immunoblotting with anti-GFP antibodies. *D*, confirmation of subcellular tethering of proteasome subunits. Cells expressing no anchor (*top panels*), the Htb2-FKBP12 nuclear anchor (*middle panels*), or the cytosol-facing plasma membrane anchor Pma1–2xFKBP12 (*bottom panels*) were pretreated for 3 h with 1 μg/ml rapamycin, at which point they were washed and transferred to SD-N media containing 1 μg/ml rapamycin, and incubated for 24 h at 30 °C. Representative micrographs of α4-GFP and Rpn11-mCherry-FRB fluorescence and merged fluorescence images are shown. *Scale bar,* 10 μm. *E,* cells expressing Rpn11-mCherry-FRB, and α4-GFP as well as either the nuclear anchor Htb2-FKBP12 (*left panel*) or the cytosol-facing plasma membrane anchor Pma1–2xFKBP12 (*right panel*) were treated with DMSO or rapamycin as indicated and described in *D* before nitrogen starvation for the indicated times. Cell extracts were prepared and subjected to immunoblotting with anti-GFP antibodies. *F*, as in *E*, but with cells expressing Rpn2-GFP instead of α4-GFP. *Asterisk*, autophagy-independent proteolytic fragment of Rpn2-GFP. This fragment was present coincident with a decrease in full-length Rpn2-GFP upon nitrogen starvation even in *atg8*Δ cells (data not shown), indicating that Rpn2-GFP may undergo some non-specific autophagy-independent proteolysis *in vivo*.

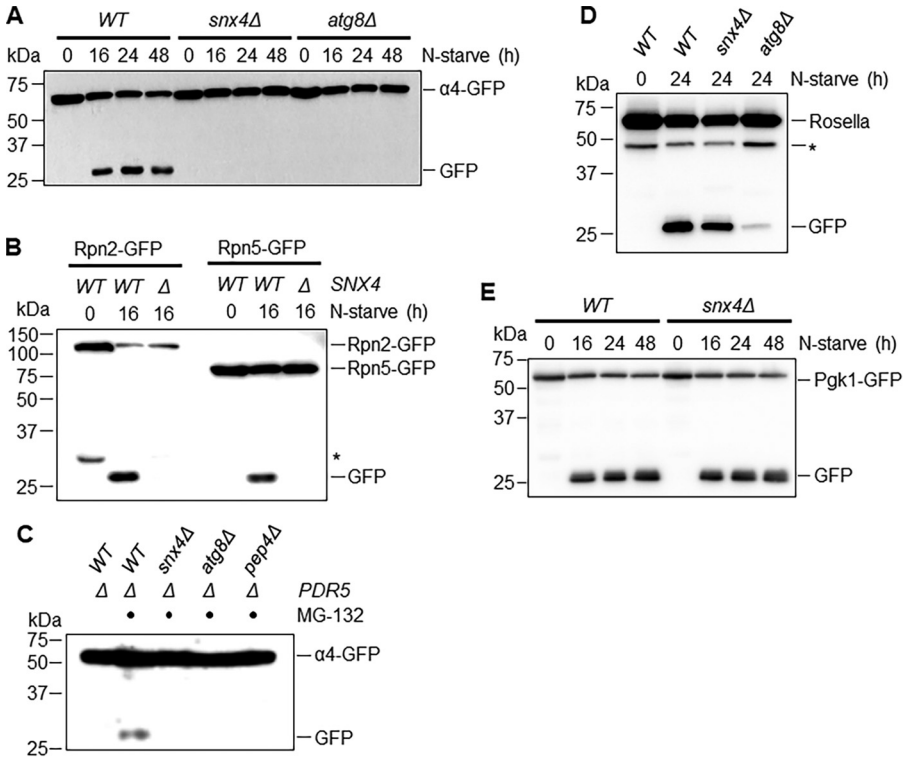

Figure 4. Snx4 is required for selective autophagy of the proteasome. *A,* indicated yeast strains were nitrogen-starved for the times shown before harvesting and analysis of whole-cell extracts by anti-GFP immunoblotting as in Fig. 3. *B,* indicated strains were nitrogen-starved for the times shown and then subjected to anti-GFP immunoblotting. *Asterisk,* non-specific Rpn2-GFP cleavage product unrelated to autophagy. *C,* indicated yeast strains, each of which harbored a deletion of *PDR5*, were treated for 24 h with 50 μM MG132 before analysis as in *A*. Autophagy of α4-GFP in response to cellular treatment with proteasome inhibitors is also compromised in *snx4*Δ yeast. Cells were treated for the indicated times with 50 μM MG132 (*black circles*) or DMSO (*no circle*), followed by harvesting for immunoblotting with antibodies against GFP. *D* and *E,* deletion of *SNX4* does not compromise non-selective autophagy. Turnover of the bulk autophagy substrates Rosella (*D*) or Pgk1-GFP (*E*) upon nitrogen starvation in the indicated strains was assessed as in *A*. *D*, *asterisk* indicates a non-specific proteolytic product unrelated to autophagy.

rather than the previously used and pleiotropic *ERG6* mutation (16), which disrupts membrane composition and permeability. Nevertheless, formation of this GFP fragment was ablated upon deletion of *ATG8* or the vacuolar protease *PEP4*, confirming this fragment was produced via autophagy. Importantly, deletion of *SNX4* also completely compromised accumulation of GFP, indicating that Snx4 is required for proteasome autophagy in response to both nitrogen starvation and treatment with proteasome inhibitors.

We next sought to test the selectivity of Snx4 for proteasome autophagy *versus* other soluble protein cargoes. We utilized a synthetic reporter consisting of a GFP-RFP fusion, called Rosella (47), as well as a GFP fusion to an endogenous protein, Pgk1 (48), for reporters of bulk (non-selective) autophagy. In WT cells, both Rosella (Fig. 4*D*) and Pgk1-GFP (Fig. 4*E*) were efficiently cleaved to GFP in response to nitrogen starvation. Importantly, these substrates were both processed to GFP fragments as effectively in cells lacking *SNX4* as in WT cells, in agreement with previous reports that *SNX4* is dispensable for bulk autophagy (44).

Snx4 is required for autophagic turnover of other, unrelated multisubunit complexes

Recently, a requirement for *SNX4* in the turnover of the fatty-acid synthase (FAS) complex by autophagy was reported, although the mechanism was not investigated (10). As FAS is also a large, soluble, and multisubunit complex, we considered the possibility that *SNX4* represents a shared requirement for the autophagic turnover of large multisubunit complexes. To test this, we evaluated the impact of *SNX4* deletion on nitrogen starvation–induced autophagy of the FAS complex, which has a similar size to the proteasome but is localized exclusively to the cytosol. We also investigated the requirement for *SNX4* in the turnover of ribosomal large and small subunits, which are also primarily cytosolic but consist both of protein and nucleic acids. We generated strains expressing from their chromosomal loci fusions of GFP to FAS complex subunit Fas2 or the ribosomal large and small subunits Rpl25 and Rps2, respectively. All three of these genes are essential, so the viability of these strains indicates that the resultant fusion proteins assemble properly into their respective multisubunit complexes and are functional. As reported previously (10), we observed robust turnover of Fas2-GFP by autophagy after 16 h of nitrogen starvation, as evidenced by the accumulation of a GFP cleavage product. As anticipated, deletion of *SNX4* nearly completely compromised autophagic turnover of the FAS subunit Fas2-GFP in response to nitrogen starvation as gauged by loss of the diagnostic GFP fragment (Fig. 5*A*). We next tested autophagy of Rpl25-GFP (Fig. 5*B*) and Rps2-GFP (Fig. 5*C*) in response to nitrogen starvation. In WT cells, both reporters were readily cleaved to a free GFP fragment, indicating successful delivery to the vacuole. This GFP fragment was absent both for Rpl25-GFP (Fig. 5*B*) and Rps2-GFP (Fig. 5*C*) when *SNX4* was deleted, indi-

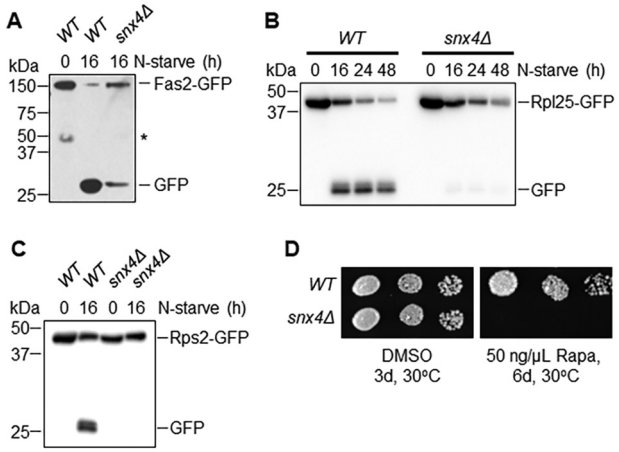

Figure 5. Snx4 is required for autophagic turnover of two other multisubunit complexes. *A*, WT or *snx4*Δ cells expressing Fas2-GFP from the chromosomal locus were nitrogen-starved for the indicated times before harvesting for SDS-PAGE and immunoblotting with anti-GFP antibodies. An *asterisk* indicates a non-specific proteolytic fragment unrelated to autophagy. *B*, as in *A* but with cells expressing the large ribosomal subunit Rpl25 as a GFP fusion instead of Fas2-GFP. *C*, as in *A* but with cells expressing the small ribosomal subunit Rps2 as a GFP fusion. *D*, equal numbers of WT or *snx4*Δ cells were spotted in 6-fold serial dilutions on YPD plates containing DMSO vehicle or 50 ng/μl rapamycin before incubation as shown and imaging.

cating a shared requirement for *SNX4* for turnover of the proteasome, FAS, and the ribosome during starvation-induced autophagy. Importantly, these three multisubunit complexes have distinct subcellular distributions (49), are composed of different macromolecules (*e.g.* proteins *versus* proteins and nucleic acids), and apparently share only their large size and multisubunit nature in common. This suggests *SNX4* may be uniformly required for selective autophagy of macromolecular complexes. In agreement with an important role in the regulated turnover of several essential multisubunit complexes, cells lacking *SNX4* displayed a severe growth defect compared with WT cells in the presence of a low concentration of the starvation mimetic rapamycin (Fig. 5*D*).

Snx4 functions prior to vacuolar delivery of α4-GFP and promotes the accumulation of cytoplasmic proteasome puncta when autophagosome formation is disrupted

We next investigated the function of Snx4 in α4-GFP autophagy via microscopy. We first asked whether α4-GFP arrived in the vacuole in nitrogen-starved *snx4*Δ cells. For this, we stabilized the protein contents of the vacuole by utilizing cells in which the gene encoding the major vacuolar peptidase, *PEP4*, had been deleted. A pattern of bright nuclear and diffuse cytosolic fluorescence typical of proteasomes (18, 19) was observed in unstarved cells (data not shown) and was generally retained upon nitrogen starvation (Fig. 6*A*). Importantly, GFP fluorescence accumulated in the vacuole (circumscribed by the vacuolar membrane protein Vph1-mCherry) upon nitrogen starvation (Fig. 6*A*). In contrast, the GFP fluorescence intensity was much lower in the vacuole of nearly all *snx4*Δ cells. Quantitative vacuolar fluorescence analysis confirmed this observation (Fig. 6*B*), suggesting the defect in *snx4*Δ cells precedes vacuolar delivery. Furthermore, we observed a slight but significant increase in the nuclear fluorescence intensity in nitrogen-starved *snx4*Δ cells, consistent with a compromise of proteasome autophagy (Fig. 6*B*).

We next examined the localization of α4-GFP upon nitrogen starvation in *atg8*Δ cells, which are compromised for autophagosome formation (50). Interestingly, we observed the presence of cytoplasmic GFP puncta in *atg8*Δ cells (Fig. 6*C*), similar to those previously observed by others in *atg17*Δ cells (17). Although they were rare, we occasionally observed such puncta in *ATG8* WT cells (not shown and Fig. 6*D*). The accumulation of these species in *atg8*Δ cells suggests that they are normally transient and were accumulating when autophagosome formation was compromised via *ATG8* deletion. In contrast to the PAS, which is invariantly perivacuolar in yeast, these puncta were often juxtanuclear and clearly separated from the vacuole in *atg8*Δ cells (Fig. 6*C*, *arrowhead*). However, they did not colocalize with the PAS or with known perinuclear structures such as the juxtanuclear quality control compartment (51) or the spindle pole body (data not shown). Importantly, these puncta were nearly completely absent in *snx4*Δ cells (Fig. 6, *C* and *D*), indicating that their accumulation requires Snx4. This dependence on Snx4 did not reflect a non-specific consequence of disrupting endosomal sorting because deletion of the *VPS35* gene, which encodes the cargo-binding subunit of the retromer complex essential for retromer-dependent endosomal sorting (52), did not affect accumulation of these puncta (Fig. 6, *C* and *D*). Thus, Snx4 mediates the formation of cytoplasmic puncta that accumulate when autophagy is impaired. Furthermore, the presence of these puncta at low frequency in WT cells, coupled with the impaired delivery of α4-GFP to the vacuole in *snx4*Δ cells (Fig. 6, *A* and *B*), suggests that Snx4 may promote the formation of these puncta for subsequent Atg8-dependent delivery to the vacuole.

Snx4 cooperates with both Snx41 and Snx42 to mediate proteasome autophagy

SNX4 family nexins typically function as dimers. In budding yeast, Snx4 can heterodimerize with two other PX-BAR family nexins, Snx41 and Snx42, to form Snx4-Snx41 and Snx4-Snx42 complexes with distinct and overlapping functions (37, 40, 41, 43). In *S. cerevisiae*, Snx4 cooperates with Snx41 to promote retrograde sorting of the autophagy integral membrane protein Atg27, whereas Snx42 is dispensable (37). In contrast, Snx4 and Snx42 cooperate to promote autophagy of peroxisomes and mitochondria (45) and is also required for the CVT pathway (44). Deletion of the *Schizosaccharomyces pombe* homologs of Snx4, Snx41, or Snx42 alone has no impact on nitrogen starvation–induced autophagy of ER or mitochondria, but deletion of select combinations of these factors compromises autophagy of these organelles (43).

To investigate whether Snx4 functions with Snx41 and/or Snx42 in proteasome autophagy, we created strains harboring single deletions of *SNX41* and *SNX42*, as well as a double deletion strain lacking both genes. We then introduced the *PRE6-GFP* allele into these deletion strains, and we assessed the impact on α4-GFP autophagy in response to nitrogen starvation. Deletion of *SNX41* alone had no measurable effect on α4-GFP autophagy as ascertained by accumulation of the GFP fragment upon nitrogen starvation, whereas deletion of *SNX42*

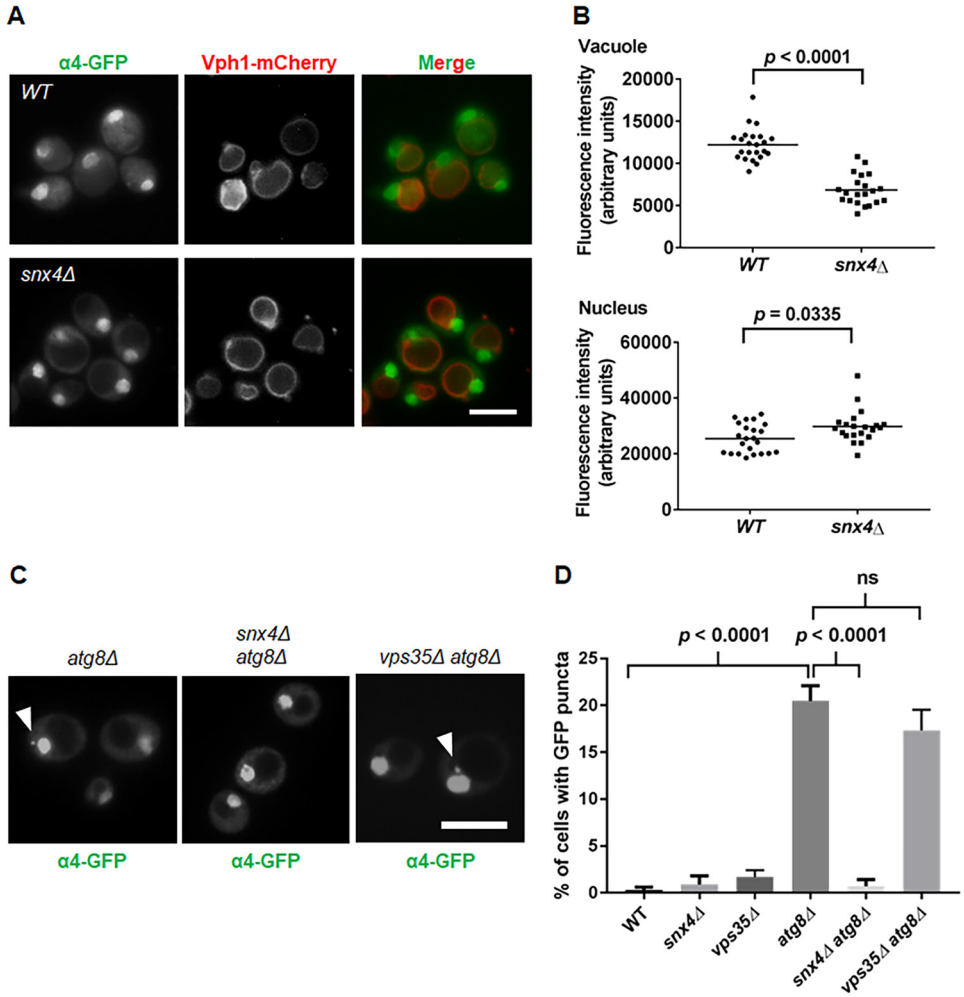

Figure 6. Snx4 is required for the formation of cytoplasmic α4-GFP puncta. *A*, WT or *snx4*Δ cells expressing α4-GFP and Vph1-mCherry (as a vacuolar membrane marker) were nitrogen-starved for 16 h before imaging. All strains lacked the vacuolar peptidase *PEP4* to stabilize vacuolar contents. Representative micrographs are shown. *Scale bar*, 5 μm. *B*, statistical dot-plot with means (*black bars*) of the intensity of GFP signal from the vacuole (*left*) or nucleus for *WT* (n = 23) and *snx4*Δ (n = 21) cells (two-tailed Mann-Whitney test). *C*, indicated strains expressing α4-GFP were nitrogen-starved for 16 h before imaging. Representative micrographs of *atg8*Δ, *snx4*Δ *atg8*Δ, or *vps35*Δ *atg8*Δ cells expressing α4-GFP are shown. *White arrowheads* indicate GFP puncta. *Scale bar*, 5 μm. *D*, quantification of cytoplasmic α4-GFP puncta in the indicated strains after nitrogen starvation for 16 h (n > 100 cells; one-way ANOVA with Tukey's test for multiple comparisons; *error bars*, S.E.). *ns*, not significant.

alone caused a small but reproducible defect when autophagy was induced in cells first grown in rich media (Fig. 7*A*). This effect was consistently less pronounced in cells grown in minimal media (Fig. 7*B* and not shown). Importantly, codeletion of *SNX41* and *SNX42* caused a complete loss of proteasome autophagy upon nitrogen starvation (Fig. 7*A*), indicating that these genes function redundantly with one another. Overexpression of Snx4 in *snx41*Δ *snx42*Δ cells failed to restore α4-GFP autophagy (Fig. 7*B*), supporting a model where Snx4 functioned in the same pathway as Snx41 and Snx42, as Snx4-Snx41 and Snx4-Snx42 heterodimers. Such a redundant function for Snx4-Snx41 and Snx4-Snx42 also rationalizes the complete compromise of proteasome autophagy in *snx4*Δ cells or when both *SNX41* and *SNX42* were deleted, but not in single *snx41*Δ or *snx42*Δ mutants (Fig. 7*A*).

To better understand the relationship between Snx4, Snx41, Snx42, and proteasome autophagy, we investigated the effect of *SNX41* and *SNX42* deletion on Snx4 subcellular localization. We expressed Snx4-GFP from the chromosomal locus and verified that this allele was functional (Fig. 7*C*). In nitrogen-starved WT cells expressing Snx4-GFP, we observed primarily cytoplasmic puncta of Snx4 (Fig. 7*D*), as is typical of endosomal proteins and as has recently been reported by others (37). We were unable to detect colocalization of mCherry-tagged proteasome subunits with these cytoplasmic Snx4-GFP puncta in *atg8*Δ cells (data not shown), indicating they are either distinct structures from the α4-GFP puncta (Fig. 6*C*) or possibly that they colocalize transiently or only rarely. Nonetheless, deletion of *SNX41* alone had no apparent effect on the appearance of Snx4-GFP puncta (Fig. 7*D*) and no statistically significant effect on their frequency (Fig. 7*E*); this was in agreement with the robust α4-GFP autophagy observed in *snx41*Δ cells (Fig. 7*A*). In contrast, deletion of *SNX42* alone caused a small but reproducible decrease in the frequency of Snx4-GFP puncta (Fig. 7*E*) and the concomitant appearance of diffuse cytoplasmic fluorescence in most cells (Fig. 7*D*), again consistent with the partial loss of α4-GFP autophagy in this mutant (Fig. 7*A*). Importantly, codeletion of *SNX41* and *SNX42* resulted in a near-complete

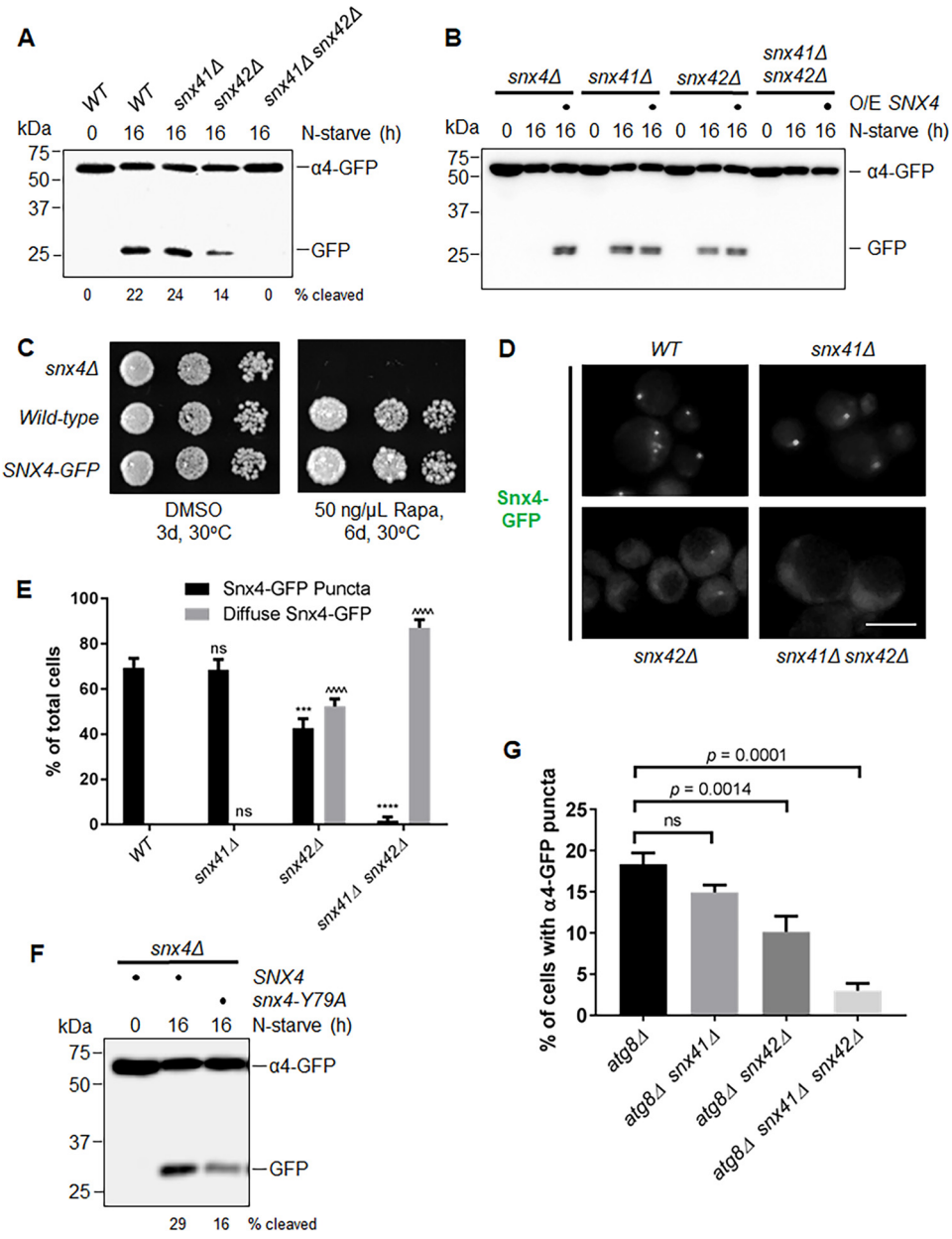

Figure 7. Snx4 cooperates with Snx41 and Snx42 to promote autophagy of proteasomes. *A*, indicated strains were nitrogen-starved, followed by analysis of whole-cell extracts by SDS-PAGE and immunoblotting with anti-GFP antibodies. The percentage of GFP fragment is shown as % cleaved. *B*, overexpression of *SNX4* fails to rescue the autophagy defect in *snx41Δ snx42Δ* cells. The indicated cells were transformed with either empty plasmid (*no circles*) or a plasmid that overproduces *SNX4*. Cells were then nitrogen-starved or not as indicated, followed by analysis of whole-cell extracts as in *A*. *C*, *SNX4-GFP* is functional. Equal numbers of the indicated cells were spotted in 6-fold serial dilutions on YPD plates containing DMSO vehicle or 50 ng/μl rapamycin before incubation as shown and imaging. *D*, micrographs of Snx4-GFP fluorescence in the indicated strains after nitrogen starvation for 16 h. *Scale bar,* 5 μm. *E*, analysis of punctate or diffuse Snx4-GFP localization (two-way ANOVA; *error bars,* S.E.). *ns,* not significantly different from WT; ***, $p = 0.0007$ *versus* WT; ****, $p < 0.0001$ *versus* WT; ^^^^, $p < 0.0001$ *versus* WT. *F*, *snx4Δ* cells were transformed with plasmids expressing either *SNX4* or *snx4*(*Y79A*) from the endogenous *SNX4* promoter. Transformants were then subjected to nitrogen starvation and analysis of whole-cell extracts by anti-GFP immunoblotting as in *A*. The percentage of GFP fragment is shown as % cleaved. *G*, quantification of cytoplasmic α4-GFP puncta in the indicated strains after nitrogen starvation for 16 h ($n > 100$ cells; one-way ANOVA with Tukey's test for multiple comparisons; *error bars,* S.E.).

loss of Snx4-GFP puncta and a further increase in diffuse cytoplasmic fluorescence (Fig. 7, *D* and *E*). This strongly suggests that proper localization of Snx4 to such puncta is important for proteasome autophagy.

Snx4 localizes to membranes via its PI3P-binding PX domain, and mutation of a critical tyrosine residue in this domain to alanine (Y79A) has previously been shown to disrupt PI3P binding and cause partial mislocalization of Snx4 (44). We thus tested the impact of this mutation on α4-GFP autophagy. We introduced plasmids expressing either WT *SNX4* or the *snx4*(*Y79A*) PX domain mutant into *snx4*Δ cells. As expected, provision of WT *SNX4* to *snx4*Δ cells restored turnover of α4-GFP upon nitrogen starvation. In contrast, provision of the *snx4*(*Y79A*) mutant restored α4-GFP autophagy to only ~50% of that observed with the WT *SNX4* allele (Fig. 7*F*). Taken together, these results indicate that Snx41 and Snx42 promote proper localization of Snx4 to perivacuolar puncta and that disruption of this localization, either via reducing PI3P binding by

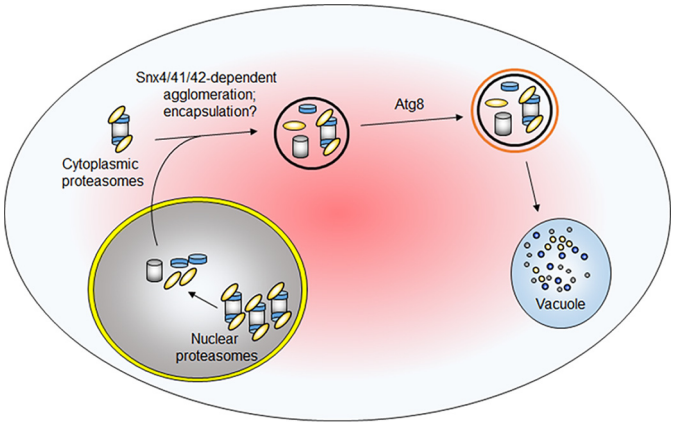

Figure 8. Model for delivery of proteasomes to the vacuole for destruction. The data support a model in which nuclear proteasomes are disassembled prior to autophagy and within the nucleus, whereas cytoplasmic proteasomes remain intact. Snx4 promotes the agglomeration of proteasomes into cytoplasmic puncta that accumulate in a step prior to Atg8-dependent encapsulation in the autophagosomal membrane (*orange circle*). Although the model depicts these Snx4-dependent puncta as membrane-enclosed (*black circle*), it is not yet clear if this is the case. Atg8 then mediates traditional encapsulation in the autophagosomal membrane for delivery to and destruction in the vacuole.

Snx4 or by disrupting formation of Snx4-containing heterodimers, compromises proteasome autophagy. Consistent with this model, codeletion of *SNX41* and *SNX42* severely compromised formation of Snx4-dependent cytoplasmic α4-GFP puncta in *atg8*Δ cells upon nitrogen starvation (Fig. 7*G*). We note that the relative loss of α4-GFP puncta in *snx41*Δ, *snx42*Δ, or *snx41*Δ *snx42*Δ cells closely mirrored the impact both on α4-GFP autophagy (Fig. 7*A*) and delocalization of Snx4-GFP (Fig. 7*E*). Thus, we conclude that Snx4 cooperates with Snx41 and Snx42 to drive the formation of cytoplasmic proteasome puncta, likely *en route* to the vacuole for destruction, in a manner dependent on proper localization of Snx4 to PI3P-containing membranes.

Discussion

Here, we provide some of the first insights into the subcellular trafficking of proteasomes to the vacuole for autophagy. We demonstrate that nuclear proteasomes can be disassembled prior to autophagy, and that proteasome autophagy is independent of known nucleophagy genes and is impaired when Crm1-dependent nuclear export is compromised. Turnover of proteasomes is completely compromised by loss of Snx4, which mediates the agglomeration of proteasomes into cytoplasmic puncta prior to delivery to the vacuole (Fig. 8). These data support a model in which autophagic turnover of nuclear and cytoplasmic proteasomes converge at the stage of Snx4-dependent agglomeration prior to delivery to the vacuole for destruction. Importantly, Snx4 mediates the turnover of diverse multisubunit complexes (Fig. 5), including the ribosome and FAS, indicating it is broadly involved in selective autophagy of soluble multisubunit complexes.

In yeasts and many mammalian cells, a substantial portion of mature proteasomes is located in the nucleus, an organelle that was generally considered to be spared from autophagic destruction until only recently. Although autophagy of proteasomes has been reported in yeast, plants, and mammals, whether nuclear and cytoplasmic proteasomes were recognized and processed via the same mechanism was not known. Our data suggest that in yeast, nuclear proteasomes are disassembled prior to autophagy (Figs. 2 and 8). These findings are consistent with recent reports that at least some fraction of proteasomes are disassembled prior to nitrogen starvation–induced autophagy (17). Why some nuclear autophagy substrates are turned over via nucleus-specific selective autophagy pathways such as PMN or Atg39-dependent nucleophagy whereas others may be independent is thus far unknown, but it may allow greater control over turnover of particular sets of nuclear autophagic substrates. Alternatively, some feature(s) of the substrate, such as membrane embedment or association, may necessitate a particular route of delivery to the vacuole from the nucleus.

Our findings that autophagic turnover of both the RP base and the CP are unaffected when the lid is tethered to chromatin suggests that, at minimum, the lid dissociates from the base and CP during autophagy of nuclear proteasomes. We suspect that all three subcomplexes dissociate from one another. In support of this, we observed different amounts of GFP liberated from lid, base, and CP subunits upon nitrogen starvation (Fig. 1, *F–H*, permissive temperature), and different requirements for autophagy of the base subunit Rpn1 and the CP subunit β5 were reported by others (17). The reason for disassembly of nuclear but not cytoplasmic proteasomes prior to autophagy is unknown. Although export through the nuclear pore has not to our knowledge been demonstrated for the proteasome, fully assembled proteasomes have been reported to pass intact through the nuclear pore into the nucleus (32, 53), arguing against the possibility that proteasomes cannot otherwise fit. Instead, we suggest that this disassembly may be necessary to limit a sudden influx of proteasome activity into the cytosol prior to autophagic engulfment that could otherwise disrupt cellular processes. Indeed, the activities of individual proteasomal subcomplexes are much lower than in the holocomplex (54, 55). Thus, such dissociation into subcomplexes may serve to inactivate or attenuate these proteasomes until they can be encapsulated by the autophagosome and shielded from cytosolic proteasome substrates.

An additional question arising is the nature of the signal for disassembly of nuclear proteasomes upon nitrogen starvation–induced autophagy. Although the interaction between the RP base and the CP has been demonstrated to be sensitive to ATP levels *in vitro* (56), nitrogen starvation does not impact the intracellular ATP concentration, at least in yeast (57, 58). Also, we are not aware of any evidence that lid and base subcomplexes dissociate in a nucleotide-dependent manner. Furthermore, such a nucleotide-dependent disassembly would be anticipated to similarly affect cytosolic proteasomes. Instead, we speculate that a nucleus-specific signal promotes disassembly of these subcomplexes. Phosphorylation may be a likely candidate. We note that nitrogen starvation regulates the activity as well as the subcellular localization of several kinases (59). Furthermore, phosphorylation has recently been shown to recruit the proteasome-binding protein Ecm29 (60), which disassembles proteasomes in response to other stimuli (61).

Based on the loss of α4-GFP puncta in *snx4*Δ cells, we propose that Snx4 is involved either in the clustering of soluble

proteasomes into phase-separated granules similar to those observed in response to carbon deprivation (62) or is instead involved in the enrichment of proteasomes in membrane-encased structures that are subsequently undergoing Atg8-dependent engulfment and delivery to the vacuole. Considering that Snx4 is a PI3P-binding protein involved in membrane protein sorting (37, 40, 41) and that its membrane-binding function is necessary for proteasome autophagy (Fig. 7), we favor the latter possibility. Indeed, while this manuscript was being prepared, a computational clustering study proposed a role for Snx4 in the membrane engulfment of selective autophagy cargos (63), although the relationship to Atg8-dependent autophagosomal membrane expansion is not yet known.

Although bulk and selective autophagy pathways share the core autophagy machinery, differences have emerged in the requirements for auxiliary factors for individual cargoes. For example, deletion of *SNX4* alone has no effect on starvation-induced autophagy of the vacuolar enzyme Ape1 (64), on organelle autophagy (43), or on bulk autophagy (Fig. 4, *D* and *E*), whereas codeletion of *SNX42* with *SNX4* compromises turnover both of Ape1 and organelles. In contrast, deletion of *SNX4* alone completely compromises autophagy of proteasomes and two other large macromolecular complexes, the FAS complex and the ribosome (Fig. 5). This suggests that these cargoes may be differentially dependent on Snx4-containing heterodimers. The mechanistic basis for this remains to be determined, but individual roles for Snx4-Snx41 and Snx4-Snx42 complexes are emerging and are likely to provide additional insight.

The underlying function of Snx4 in proteasome autophagy, as well as in other forms of selective autophagy, remains unclear. Numerous studies have documented a contribution of the endosomal sorting machinery to selective autophagy (65), and early endosomal markers have been observed in autophagic vesicles (66). Specifically, roles in membrane delivery to the autophagosome from the Golgi (64) and trafficking of autophagy proteins (37) have been proposed for Snx4. However, each of these roles required deletion of multiple genes to manifest a defect in selective autophagy of other cargoes. Our finding that deletion of *SNX4* completely compromised proteasome autophagy suggests a more central role for Snx4 in this process. We have anecdotally observed that the α4-GFP puncta that accumulate in *atg8*Δ cells are often juxtaposed to the early endosome marker mCherry-Tlg1,[4] raising the intriguing possibility that Snx4 may mediate engulfment of proteasomes at the endosome or instead may promote extrusion of proteasomes destined for the vacuole from the endosomal compartment. The direct delivery of cargo to the autophagosome from early endosomes via vesicle fusion is not entirely unprecedented (66, 67). Our observation that any perturbations that disrupt Snx4 localization also compromise proteasome autophagy (Fig. 7) is consistent with this hypothesis. Live-cell microscopy studies will be necessary to determine whether proteasomes pass through the endosome *en route* to the vacuole. Furthermore, identification of additional genes necessary for the accumulation of α4-GFP puncta in *atg8*Δ cells will provide valuable insight into the origin of these species, as well as into the mechanism of Snx4-dependent cargo processing for autophagy.

[4] A. A. Nemec, L. A. Howell, A. K. Peterson, M. A. Murray, and R. J. Tomko, Jr., unpublished results.

Experimental procedures

Yeast strains and media

Yeast manipulations were carried out according to standard protocols (68). Strains used in this study are listed in supplemental Table S1. For nitrogen starvation, yeast were grown in YPD or synthetic dropout medium to mid-log, centrifuged at 4000 × *g* for 2 min, washed once with 15 ml of distilled H_2O, centrifuged again, and then resuspended to an A_{600} of 1.0 in SD-N media (0.67% yeast nitrogen base without amino acids or ammonium sulfate, 2% glucose). For temperature shift experiments using the *xpo1-1* allele, cells were grown at 25 °C and subjected to nitrogen starvation as above. After 3 h, cultures were split in two; one-half continued to be incubated at 25 °C, and the other half was subsequently incubated at 37 °C to inactivate the *xpo1-1* mutant allele. Where indicated, mid-log phase yeast grown in YPD were treated with 50 μM MG132 in DMSO as described in the figure legends. For anchor-away experiments, yeast were grown to mid-log in YPD, and then treated for 3 h with 1 μg/ml rapamycin (Enzo Life Sciences) prior to nitrogen starvation as above in SD-N supplemented with 1 μg/ml rapamycin. For growth assays, the indicated strains were spotted as 6-fold serial dilutions in water onto the indicated media.

Plasmids

All plasmids were constructed using standard molecular cloning techniques using TOP10 F′ (Invitrogen) as a host strain. Plasmids used in this study are listed in supplemental Table S2. Complete sequences and construction details are available upon request.

Genetic array analysis

ATG deletion strains were hand-picked from the YKO library (Open Biosystems) and arrayed in a 96-well format. A query strain derived from Y7092 (34) was produced by sequentially integrating *PRE6-yEGFP:caURA3MX4* and *pdr5*Δ*::natMX4* cassettes into the respective chromosomal loci. After confirmation of integration, this resultant query strain (RTY1207) was mated to the *ATG* deletion array to generate haploid triple mutant strains. The presence of the *pdr5*Δ allele did not affect nitrogen starvation–induced autophagy of α4-GFP in our hands.

SDS-PAGE and immunoblotting

Cell extracts were prepared from equal numbers of cells via the alkaline lysis method (69) and cleared via centrifugation. The supernatants were loaded directly onto 12% SDS-polyacrylamide gels. After electrophoresis, proteins were transferred to PVDF membranes (EMD Millipore) and probed with antibodies against GFP (Roche Applied Science, catalog no. 11814460001, 1:2000 dilution). Blots were imaged on an Azure Biosystems c300 or a Bio-Rad ChemiDoc MP using HRP-conjugated secondary antibodies (GE Healthcare, catalog no. 95017-332, 1:5000) and ECL reagent. The percentage of free

GFP liberated from a given protein was calculated for each sample by dividing the band intensity from the free GFP product by the sum of the intensities of free GFP plus the intact GFP fusion protein and thus is internally normalized across sample lanes. Band intensities were confirmed to be in the linear signal range using ImageLab software (Bio-Rad) and were quantified from raw image files. GFP cleavage measurements reported in the figures are of the blot shown, but are representative of multiple experiments.

Non-denaturing PAGE of cell extracts and fluorescence analyses

Cell extracts (100 μg of total protein) were separated by non-denaturing PAGE exactly as described previously (70). To visualize in-gel GFP fluorescence, gels were washed once in deionized water after electrophoresis and were imaged with a Typhoon Imager (GE Healthcare) using excitation at 488 nm, and measurement of emission through a 520-nm bandpass filter. For measurement of suc-LLVY-AMC hydrolysis, non-denaturing gels in which 100 μg of cell extract had been separated were incubated in Overlay buffer (50 mM Tris-Cl, pH 7.5, 5 mM $MgCl_2$, 10% glycerol, 1 mM ATP) containing 50 μM suc-LLVY-AMC for 30 min at 30 °C with occasional gentle agitation. Liberated AMC was detected in a Bio-Rad Gel-doc XR imaging system with the pre-programmed excitation and emission settings for ethidium bromide. For anti-20S immunoblotting, 50 μg of cell extract was separated exactly as above before transfer to PVDF membranes and immunoblotting with anti-20S antibodies (Enzo, catalog no. BML-PW9355, 1:2000 dilution).

Microscopy

All micrographs were collected on an EVOS FL Cell Imaging System (Thermo Fisher Scientific) equipped with GFP and RFP filter sets. Identical exposure times and light intensities were used for each image in a given experiment. Briefly, cells were collected via centrifugation at 10,000 $\times$ *g* for 30 s, followed by resuspension in the appropriate medium at 1/10th of the original culture volume. To minimize cell movement during imaging, pre-cleaned microscope slides were overlaid with a thin pad of 3% agarose containing the appropriate culture medium onto which the cells were applied. In Fig. 6*B*, vacuolar or nuclear fluorescence intensity was measured using ImageJ on raw image files, and individual cell measurements were plotted.

Statistical analysis and reproducibility

All experiments were performed three times or more to ensure reproducibility. Statistical analysis was carried out using Graph Pad Prism 7.0 software, via two-tailed Mann-Whitney test (Fig. 6*B*), one-way ANOVA with Tukey's test for multiple comparisons (Fig. 6*D*), two-way ANOVA with Sidak's test for multiple comparisons (Fig. 7*E*), or one-way ANOVA with Dunnett's test for multiple comparisons (Fig. 7*G*). Unless otherwise indicated, at least 100 cells per condition were analyzed for statistical analysis of micrographs. Statistical significance was considered $p < 0.05$.

Author contributions—A. A. N. and R. J. T., Jr. conceived and designed the study. Most experiments were replicated by more than one author. L. A. H. performed or contributed reagents to Figs. 1, *D–H*, 2, 6, and 7. A. A. N. performed experiments in Figs. 1*C*, 2–4, and 6, *C* and *D*. A. K. P. contributed reagents to all figures and helped conduct the screen in Fig. 3. M. A. M. performed experiments in Fig. 5. R. J. T., Jr. contributed reagents and performed experiments in Figs. 1*B*, and 6, *A* and *B*. R. J. T., Jr. wrote the manuscript with input from all authors.

Acknowledgments—We thank Rodney Devenish (Monash University), Akash Gunjan (Florida State University College of Medicine), and Daniel Klionsky (University of Michigan) for reagents, and the Florida State University yeast community for helpful comments and feedback.

References

1. Cohen-Kaplan, V., Livneh, I., Avni, N., Cohen-Rosenzweig, C., and Ciechanover, A. (2016) The ubiquitin–proteasome system and autophagy: coordinated and independent activities. *Int. J. Biochem. Cell Biol.* **79,** 403–418
2. Finley, D. (2009) Recognition and processing of ubiquitin-protein conjugates by the proteasome. *Annu. Rev. Biochem.* **78,** 477–513
3. Tomko, R. J., Jr., and Hochstrasser, M. (2013) Molecular architecture and assembly of the eukaryotic proteasome. *Annu. Rev. Biochem.* **82,** 415–445
4. Feng, Y., He, D., Yao, Z., and Klionsky, D. J. (2014) The machinery of macroautophagy. *Cell Res.* **24,** 24–41
5. Welter, E., and Elazar, Z. (2015) Autophagy mediates non-selective RNA degradation in starving yeast. *EMBO J.* **34,** 131–133
6. Jaishy, B., and Abel, E. D. (2016) Lipids, lysosomes, and autophagy. *J. Lipid Res.* **57,** 1619–1635
7. Anding, A. L., and Baehrecke, E. H. (2017) Cleaning house: selective autophagy of organelles. *Dev. Cell* **41,** 10–22
8. Wileman, T. (2013) Autophagy as a defence against intracellular pathogens. *Essays Biochem.* **55,** 153–163
9. Kraft, C., Deplazes, A., Sohrmann, M., and Peter, M. (2008) Mature ribosomes are selectively degraded upon starvation by an autophagy pathway requiring the Ubp3p/Bre5p ubiquitin protease. *Nat. Cell Biol.* **10,** 602–610
10. Shpilka, T., Welter, E., Borovsky, N., Amar, N., Shimron, F., Peleg, Y., and Elazar, Z. (2015) Fatty acid synthase is preferentially degraded by autophagy upon nitrogen starvation in yeast. *Proc. Natl. Acad. Sci. U.S.A.* **112,** 1434–1439
11. Le Fourn, V., Park, S., Jang, I., Gaplovska-Kysela, K., Guhl, B., Lee, Y., Cho, J. W., Zuber, C., and Roth, J. (2013) Large protein complexes retained in the ER are dislocated by non-COPII vesicles and degraded by selective autophagy. *Cell. Mol. Life Sci.* **70,** 1985–2002
12. Mizushima, N., Levine, B., Cuervo, A. M., and Klionsky, D. J. (2008) Autophagy fights disease through cellular self-digestion. *Nature* **451,** 1069–1075
13. Stolz, A., Ernst, A., and Dikic, I. (2014) Cargo recognition and trafficking in selective autophagy. *Nat. Cell Biol.* **16,** 495–501
14. Cohen-Kaplan, V., Livneh, I., Avni, N., Fabre, B., Ziv, T., Kwon, Y. T., and Ciechanover, A. (2016) p62- and ubiquitin-dependent stress-induced autophagy of the mammalian 26S proteasome. *Proc. Natl. Acad. Sci. U.S.A.* **113,** E7490–E7499
15. Marshall, R. S., Li, F., Gemperline, D. C., Book, A. J., and Vierstra, R. D. (2015) Autophagic degradation of the 26S proteasome is mediated by the dual ATG8/ubiquitin receptor RPN10 in *Arabidopsis*. *Mol. Cell* **58,** 1053–1066
16. Marshall, R. S., McLoughlin, F., and Vierstra, R. D. (2016) Autophagic turnover of inactive 26S proteasomes in yeast is directed by the ubiquitin receptor Cue5 and the Hsp42 chaperone. *Cell Rep.* **16,** 1717–1732

17. Waite, K. A., De-La Mota-Peynado, A., Vontz, G., and Roelofs, J. (2016) Starvation induces proteasome autophagy with different pathways for core and regulatory particles. *J. Biol. Chem.* **291,** 3239–3253
18. Enenkel, C., Lehmann, A., and Kloetzel, P. M. (1999) GFP-labelling of 26S proteasomes in living yeast: insight into proteasomal functions at the nuclear envelope/rough ER. *Mol. Biol. Rep.* **26,** 131–135
19. Enenkel, C., Lehmann, A., and Kloetzel, P. M. (1998) Subcellular distribution of proteasomes implicates a major location of protein degradation in the nuclear envelope-ER network in yeast. *EMBO J.* **17,** 6144–6154
20. Tanaka, K., Kumatori, A., Ii, K., and Ichihara, A. (1989) Direct evidence for nuclear and cytoplasmic colocalization of proteasomes (multiprotease complexes) in liver. *J. Cell. Physiol.* **139,** 34–41
21. Palmer, A., Rivett, A. J., Thomson, S., Hendil, K. B., Butcher, G. W., Fuertes, G., and Knecht, E. (1996) Subpopulations of proteasomes in rat liver nuclei, microsomes and cytosol. *Biochem. J.* **316,** 401–407
22. Brooks, P., Fuertes, G., Murray, R. Z., Bose, S., Knecht, E., Rechsteiner, M. C., Hendil, K. B., Tanaka, K., Dyson, J., and Rivett, J. (2000) Subcellular localization of proteasomes and their regulatory complexes in mammalian cells. *Biochem. J.* **346,** 155–161
23. Dou, Z., Xu, C., Donahue, G., Shimi, T., Pan, J. A., Zhu, J., Ivanov, A., Capell, B. C., Drake, A. M., Shah, P. P., Catanzaro, J. M., Ricketts, M. D., Lamark, T., Adam, S. A., Marmorstein, R., *et al.* (2015) Autophagy mediates degradation of nuclear lamina. *Nature* **527,** 105–109
24. Mijaljica, D., Prescott, M., and Devenish, R. J. (2012) A late form of nucleophagy in *Saccharomyces cerevisiae*. *PLoS One* **7,** e40013
25. Elbaz-Alon, Y., Eisenberg-Bord, M., Shinder, V., Stiller, S. B., Shimoni, E., Wiedemann, N., Geiger, T., and Schuldiner, M. (2015) Lam6 regulates the extent of contacts between organelles. *Cell Rep.* **12,** 7–14
26. Mochida, K., Oikawa, Y., Kimura, Y., Kirisako, H., Hirano, H., Ohsumi, Y., and Nakatogawa, H. (2015) Receptor-mediated selective autophagy degrades the endoplasmic reticulum and the nucleus. *Nature* **522,** 359–362
27. Klionsky, D. J., Abdelmohsen, K., Abe, A., Abedin, M. J., Abeliovich, H., Acevedo Arozena, A., Adachi, H., Adams, C. M., Adams, P. D., Adeli, K., Adhihetty, P. J., Adler, S. G., Agam, G., Agarwal, R., *et al.* (2016) Guidelines for the use and interpretation of assays for monitoring autophagy (3rd Ed.). *Autophagy* **12,** 1–222
28. Stade, K., Ford, C. S., Guthrie, C., and Weis, K. (1997) Exportin 1 (Crm1p) is an essential nuclear export factor. *Cell* **90,** 1041–1050
29. Kaake, R. M., Milenković, T., Przulj, N., Kaiser, P., and Huang, L. (2010) Characterization of cell cycle specific protein interaction networks of the yeast 26S proteasome complex by the QTAX strategy. *J. Proteome Res.* **9,** 2016–2029
30. Haruki, H., Nishikawa, J., and Laemmli, U. K. (2008) The anchor-away technique: rapid, conditional establishment of yeast mutant phenotypes. *Mol. Cell* **31,** 925–932
31. Müller, M., Schmidt, O., Angelova, M., Faserl, K., Weys, S., Kremser, L., Pfaffenwimmer, T., Dalik, T., Kraft, C., Trajanoski, Z., Lindner, H., and Teis, D. (2015) The coordinated action of the MVB pathway and autophagy ensures cell survival during starvation. *Elife* **4,** e07736
32. Pack, C. G., Yukii, H., Toh-e, A., Kudo, T., Tsuchiya, H., Kaiho, A., Sakata, E., Murata, S., Yokosawa, H., Sako, Y., Baumeister, W., Tanaka, K., and Saeki, Y. (2014) Quantitative live-cell imaging reveals spatio-temporal dynamics and cytoplasmic assembly of the 26S proteasome. *Nat. Commun.* **5,** 3396
33. Giaever, G., Chu, A. M., Ni, L., Connelly, C., Riles, L., Véronneau, S., Dow, S., Lucau-Danila, A., Anderson, K., André, B., Arkin, A. P., Astromoff, A., El-Bakkoury, M., Bangham, R., Benito, R., *et al.* (2002) Functional profiling of the *Saccharomyces cerevisiae* genome. *Nature* **418,** 387–391
34. Tong, A. H., and Boone, C. (2006) Synthetic genetic array analysis in *Saccharomyces cerevisiae*. *Methods Mol. Biol.* **313,** 171–192
35. Haft, C. R., de la Luz Sierra, M., Barr, V. A., Haft, D. H., and Taylor, S. I. (1998) Identification of a family of sorting nexin molecules and characterization of their association with receptors. *Mol. Cell. Biol.* **18,** 7278–7287
36. Gallon, M., and Cullen, P. J. (2015) Retromer and sorting nexins in endosomal sorting. *Biochem. Soc. Trans.* **43,** 33–47
37. Ma, M., Burd, C. G., and Chi, R. J. (2017) Distinct complexes of yeast Snx4 family SNX-BARs mediate retrograde trafficking of Snc1 and Atg27. *Traffic* **18,** 134–144
38. Solis, G. P., Hülsbusch, N., Radon, Y., Katanaev, V. L., Plattner, H., and Stuermer, C. A. (2013) Reggies/flotillins interact with Rab11a and SNX4 at the tubulovesicular recycling compartment and function in transferrin receptor and E-cadherin trafficking. *Mol. Biol. Cell* **24,** 2689–2702
39. Traer, C. J., Rutherford, A. C., Palmer, K. J., Wassmer, T., Oakley, J., Attar, N., Carlton, J. G., Kremerskothen, J., Stephens, D. J., and Cullen, P. J. (2007) SNX4 coordinates endosomal sorting of TfnR with dynein-mediated transport into the endocytic recycling compartment. *Nat. Cell Biol.* **9,** 1370–1380
40. Hettema, E. H., Lewis, M. J., Black, M. W., and Pelham, H. R. (2003) Retromer and the sorting nexins Snx4/41/42 mediate distinct retrieval pathways from yeast endosomes. *EMBO J.* **22,** 548–557
41. Bean, B. D., Davey, M., and Conibear, E. (2017) Cargo selectivity of yeast sorting nexins. *Traffic* **18,** 110–122
42. Maruzs, T., Lőrincz, P., Szatmári, Z., Széplaki, S., Sándor, Z., Lakatos, Z., Puska, G., Juhász, G., and Sass, M. (2015) Retromer ensures the degradation of autophagic cargo by maintaining lysosome function in *Drosophila*. *Traffic* **16,** 1088–1107
43. Zhao, D., Liu, X. M., Yu, Z. Q., Sun, L. L., Xiong, X., Dong, M. Q., and Du, L. L. (2016) Atg20- and Atg24-family proteins promote organelle autophagy in fission yeast. *J. Cell Sci.* **129,** 4289–4304
44. Nice, D. C., Sato, T. K., Stromhaug, P. E., Emr, S. D., and Klionsky, D. J. (2002) Cooperative binding of the cytoplasm to vacuole targeting pathway proteins, Cvt13 and Cvt20, to phosphatidylinositol 3-phosphate at the pre-autophagosomal structure is required for selective autophagy. *J. Biol. Chem.* **277,** 30198–30207
45. Kanki, T., Wang, K., Baba, M., Bartholomew, C. R., Lynch-Day, M. A., Du, Z., Geng, J., Mao, K., Yang, Z., Yen, W. L., and Klionsky, D. J. (2009) A genomic screen for yeast mutants defective in selective mitochondria autophagy. *Mol. Biol. Cell* **20,** 4730–4738
46. Collins, G. A., Gomez, T. A., Deshaies, R. J., and Tansey, W. P. (2010) Combined chemical and genetic approach to inhibit proteolysis by the proteasome. *Yeast* **27,** 965–974
47. Rosado, C. J., Mijaljica, D., Hatzinisiriou, I., Prescott, M., and Devenish, R. J. (2008) Rosella: a fluorescent pH-biosensor for reporting vacuolar turnover of cytosol and organelles in yeast. *Autophagy* **4,** 205–213
48. Welter, E., Thumm, M., and Krick, R. (2010) Quantification of non-selective bulk autophagy in S. cerevisiae using Pgk1-GFP. *Autophagy* **6,** 794–797
49. Huh, W. K., Falvo, J. V., Gerke, L. C., Carroll, A. S., Howson, R. W., Weissman, J. S., and O'Shea, E. K. (2003) Global analysis of protein localization in budding yeast. *Nature* **425,** 686–691
50. Kirisako, T., Baba, M., Ishihara, N., Miyazawa, K., Ohsumi, M., Yoshimori, T., Noda, T., and Ohsumi, Y. (1999) Formation process of autophagosome is traced with Apg8/Aut7p in yeast. *J. Cell Biol.* **147,** 435–446
51. Kaganovich, D., Kopito, R., and Frydman, J. (2008) Misfolded proteins partition between two distinct quality control compartments. *Nature* **454,** 1088–1095
52. Nothwehr, S. F., Ha, S. A., and Bruinsma, P. (2000) Sorting of yeast membrane proteins into an endosome-to-Golgi pathway involves direct interaction of their cytosolic domains with Vps35p. *J. Cell Biol.* **151,** 297–310
53. Savulescu, A. F., Shorer, H., Kleifeld, O., Cohen, I., Gruber, R., Glickman, M. H., and Harel, A. (2011) Nuclear import of an intact preassembled proteasome particle. *Mol. Biol. Cell* **22,** 880–891
54. Dambacher, C. M., Worden, E. J., Herzik, M. A., Martin, A., and Lander, G. C. (2016) Atomic structure of the 26S proteasome lid reveals the mechanism of deubiquitinase inhibition. *Elife* **5,** e13027
55. Groll, M., Bajorek, M., Köhler, A., Moroder, L., Rubin, D. M., Huber, R., Glickman, M. H., and Finley, D. (2000) A gated channel into the proteasome core particle. *Nat. Struct. Biol.* **7,** 1062–1067
56. Kleijnen, M. F., Roelofs, J., Park, S., Hathaway, N. A., Glickman, M., King, R. W., and Finley, D. (2007) Stability of the proteasome can be regulated allosterically through engagement of its proteolytic active sites. *Nat. Struct. Mol. Biol.* **14,** 1180–1188
57. Thomsson, E., Larsson, C., Albers, E., Nilsson, A., Franzén, C. J., and Gustafsson, L. (2003) Carbon starvation can induce energy deprivation and loss of fermentative capacity in *Saccharomyces cerevisiae*. *Appl. Environ. Microbiol.* **69,** 3251–3257

58. Nilsson, A., Påhlman, I. L., Jovall, P. A., Blomberg, A., Larsson, C., and Gustafsson, L. (2001) The catabolic capacity of *Saccharomyces cerevisiae* is preserved to a higher extent during carbon compared to nitrogen starvation. *Yeast* **18,** 1371–1381
59. Rødkaer, S. V., and Faergeman, N. J. (2014) Glucose- and nitrogen sensing and regulatory mechanisms in *Saccharomyces cerevisiae*. *FEMS Yeast Res.* **14,** 683–696
60. Wani, P. S., Suppahia, A., Capalla, X., Ondracek, A., and Roelofs, J. (2016) Phosphorylation of the C-terminal tail of proteasome subunit α7 is required for binding of the proteasome quality control factor Ecm29. *Sci. Rep.* **6,** 27873
61. Wang, X., Yen, J., Kaiser, P., and Huang, L. (2010) Regulation of the 26S proteasome complex during oxidative stress. *Sci. Signal.* **3,** ra88
62. Laporte, D., Salin, B., Daignan-Fornier, B., and Sagot, I. (2008) Reversible cytoplasmic localization of the proteasome in quiescent yeast cells. *J. Cell Biol.* **181,** 737–745
63. Kramer, M. H., Farré, J. C., Mitra, K., Yu, M. K., Ono, K., Demchak, B., Licon, K., Flagg, M., Balakrishnan, R., Cherry, J. M., Subramani, S., and Ideker, T. (2017) Active interaction mapping reveals the hierarchical organization of autophagy. *Mol. Cell* **65,** 761–774
64. Ohashi, Y., and Munro, S. (2010) Membrane delivery to the yeast autophagosome from the Golgi-endosomal system. *Mol. Biol. Cell* **21,** 3998–4008
65. Tooze, S. A., Abada, A., and Elazar, Z. (2014) Endocytosis and autophagy: exploitation or cooperation? *Cold Spring Harb. Perspect. Biol.* **6,** a018358
66. Berg, T. O., Fengsrud, M., Strømhaug, P. E., Berg, T., and Seglen, P. O. (1998) Isolation and characterization of rat liver amphisomes. Evidence for fusion of autophagosomes with both early and late endosomes. *J. Biol. Chem.* **273,** 21883–21892
67. Razi, M., Chan, E. Y., and Tooze, S. A. (2009) Early endosomes and endosomal coatomer are required for autophagy. *J. Cell Biol.* **185,** 305–321
68. Guthrie, C., and Fink, G. R. (eds) (1991) *Guide to Yeast Genetics and Molecular Biology*, Academic Press, San Diego
69. Kushnirov, V. V. (2000) Rapid and reliable protein extraction from yeast. *Yeast* **16,** 857–860
70. Tomko, R. J., Jr., and Hochstrasser, M. (2014) The intrinsically disordered Sem1 protein functions as a molecular tether during proteasome lid biogenesis. *Mol. Cell* **53,** 433–443